Self-Assembly of a Tail-End Pyridinium Polyamphiphile Complexed with *n*-Alkyl Sulfonates of Variable Chain Length

Pascal Y. Vuillaume† and C. Geraldine Bazuin*

Centre de recherche en sciences et ingénierie des macromolécules (CERSIM), Département de chimie, Université Laval, Québec, Canada G1K 7P4

Received April 7, 2003

ABSTRACT: A methylpyridinium tail-end polyamphiphile with a 12-methylene spacer was complexed with *n*-alkyl sulfonate surfactants of 4, 8, and 16 carbon lengths. The thermal and structural properties of these poly(12-methacryloyloxydodecyl-4-methylpyridinium sulfonate)s in the solid state were studied. The complexes with the two shorter surfactants self-assemble into a disordered lamellar-like morphology, with relatively short correlation lengths, similar to the parent Br-neutralized homopolymer. Two glass transition-like events are observed in the DSC thermograms and are ascribed to nanophase-separated nonionic and ionic subplanes, respectively. The complex with the longest surfactant displays thermotropic liquid crystalline behavior, with transitions between two different partially crystalline phases (related to surfactant tail-end crystallization), a smectic A-like mesophase, and the isotropic phase. Surprisingly, the lamellar spacings for all of the complexes are very similar to that of the parent polymer. Two possible structural models taking this into account are discussed.

Introduction

Self-assembly of two or more components based on noncovalent bonding interactions has become a commonly used tool in the design of macromolecular systems.[1−5] Among the increasingly large array of solid-state or bulk supramolecular polymeric systems that have been synthesized using self-assembly principles are oppositely charged polyelectrolyte−surfactant complexes.[6−9] These complexes can be thought of as simple comblike polymers where the teeth are grafted to the polymer backbone by ion-pairing. They typically organize as layered mesomorphic or liquid crystalline structures, but they do not generally display a well-defined transition to an isotropic phase, although this may occur gradually. Tail-end crystallization is observed for sufficiently long surfactants. At stoichiometric compositions, the complexes are generally insoluble in water but can be soluble in organic solvents.

We have recently synthesized a series of tail-end pyridinium-based polyamphiphiles, and studied their solid-state characteristics.[10] Like the polyelectrolyte−surfactant complexes, they tend to organize as mesomorphic disordered layer structures with no well-defined transition to an isotropic phase.[11] They possess a clear and relatively low glass transition temperature whose value depends on both the spacer length and the rigidity of the pyridinium group. The location of the ionic moiety at the end of long side chains makes them ideal components for the design of novel self-assembling complexes. They can be viewed as comblike polymers with hinges at the ends of the teeth that, when complexed with other elongated molecules, may allow backfolding or simple extension of the teeth or bends to other angles. Kato and colleagues have developed an extensive series of such materials, mainly based on hydrogen-bonding interactions between tail-end benzoic acid-functionalized side-chain polymers and pyridyl-functionalized small molecules.[3] The directionality of the hydrogen bond fixes the angle of the hinge in these materials.

In the work presented here, we have prepared ionic complexes between one of the pyridinium polyamphiphiles studied previously, namely poly(12-methacryloyloxydodecyl-4-methylpyridinium bromide) (P12MP-Br), and simple *n*-alkylsodium sulfonate surfactants of different alkyl lengths (Sp-Na, where p indicates 4, 8, or 16 carbon atoms in the alkyl chain); see Figure 1. Two of the surfactants are shorter than the alkyl spacer of the polymer and one is longer. Following ion exchange and elimination of the NaBr microions, the sulfonate surfactant becomes the polyamphiphile counterion (P12MP-Sp). These polyamphiphile−surfactant complexes are analogous to the polyelectrolyte−surfactant complexes, thus based on (nondirectional) ionic bonding, but with the complexation site far from the polymer backbone, which should enhance the polymeric character of the resulting materials. We will show, among other characteristics, that the complex with the longest surfactant displays thermotropic liquid crystalline behavior, whereas the complexes with the two shorter surfactants are simply mesomorphic like the parent polyamphiphile but give rise to two apparent glass transition temperatures.

Experimental Section

Materials. Sodium butylsulfonate (S4-Na; Aldrich, 98%), sodium octylsulfonate (S8-Na; Aldrich, 98%), sodium hexadecylsulfonate (S16-Na; Acros, 98%), and 2-mercaptoethanol (ME; Aldrich) were used as received. Dialysis membranes (SpectraPor, VWR) had a nominal cutoff of 6000−8000 Da. All solvents used were of analytical grade. Water used for polymerization and dialysis was purified by a Barnstead Nanopure II water purification system (resistance 18.2 MΩ).

Techniques. Elemental analysis, energy-dispersive X-ray microanalysis (EDX) coupled to a scanning electron microscope (SEM), and nuclear magnetic resonance spectroscopy (NMR)

* To whom correspondence should be addressed. Address as of June 1, 2003: Département de chimie, Université de Montréal, C. P. 6128 Succursale Centre-Ville, Montréal (QC), Canada H3C 3J7.

† Current address: Faculté de médecine vétérinaire, Université de Montréal, 3200 rue Sicotte, Saint-Hyacinthe (QC), Canada J2S 7C6.

10.1021/ma0344442 CCC: $25.00
Published on Web 08/01/2003

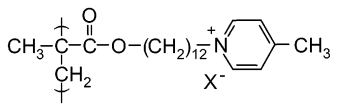

P12MP-Br, $X^- = Br^-$

P12MP-Sp, $X^- = C_pH_{2p+1}SO_3^-$ (p = 4, 8,16)

Figure 1. Chemical structure and acronyms of the polyamphiphiles (P12MP-Br) and polyamphiphile−surfactant complexes (P12MP-Sp).

were used to verify the composition and purity of the prepared complexes. Elemental analysis of the elements, C, H, N, O, S and Br, was performed at Institut Charles Sadron (Strasbourg, France): C, H, N and S were analyzed using a Carlo Elba Elemental analyzer, model 1106, the direct dosage of oxygen was performed according to a procedure described elsewhere,[12] and the bromide ions were titrated in methanol by silver nitrate using a Mettler DL21 potentiometer. EDX-SEM analysis was performed using a JEOL JSM-840A apparatus equipped with a LaB_6 monocrystal, with the samples coated by a Au/Pd alloy; this allowed the completeness of ion exchange in the complexes to be verified by the absence of Na and Br signals at 1.0 and 1.5 keV, respectively. NMR spectra were obtained with a 300 MHz Bruker spectrometer; chemical shifts, δ, are given in ppm relative to the solvent residual resonances fixed at 7.27 and 4.61 ppm for $CDCl_3$ and D_2O, respectively.

Thermogravimetric analysis (TGA) was carried out under constant nitrogen flow (200 mL·min^{-1}) at a heating rate of 5 °C/min using a Mettler TA 3000 TGA. The samples were previously dried in vacuo at 60 °C and then in situ at 80 °C for 10 min just prior to the heating scans. The temperature of thermal degradation was determined as the point of 5% weight loss relative to the weight at 80 °C.

Differential scanning calorimetry (DSC) was performed using a Perkin-Elmer DSC-7 calorimeter calibrated with indium and flushed with He. Surfactant samples were dried overnight at 90 °C in vacuo; about 8 mg was packed in standard aluminum pans and scanned at 10 °C/min. Samples of the complexes (8−18 mg) were dried in vacuo at ca. 100 °C for 2 days (unless otherwise mentioned), packed in aluminum pans with previously pierced covers, and scanned at 20 °C/min. First-order transition temperatures are given by the peak values. Glass transition temperatures (T_g) are given as the midpoint of the heat capacity jump. The data reported are averages obtained from several scans of two or more samples. All scans were reproducible after the initial heating scan, with the T_g frequently being a few degrees lower on the first scan compared to the subsequent scans. In a dynamic DSC (DDSC) experiment, 80 heat-cool cycles with rates of 8 and 4 °C/min, respectively, were applied.

Polarizing optical microscopy (POM) observations of the samples were made using a Zeiss Axioskop microscope equipped with a 25× Leica objective, a Mettler FP5 temperature controller, and a FP52 hot stage.

X-ray diffractometry (XRD) was carried out using two different diffractometers. With the Rigaku apparatus (used for the data presented in Figures 5 and 7), nickel-filtered Cu Kα radiation was produced by a rotating anode X-ray generator (Rotaflex RU-200BH) operated at 55 kV and 190 mA, and collimation was effected by a Soller slit and a 1 mm pinhole. The diffraction profiles, for 2θ angles varying between 1.1 and 30 deg, were scanned by a scintillation counter (SC-30) coupled to a pulse-height analyzer. Temperature was controlled by a homemade water-cooled copper block oven. With the Bruker apparatus (used for the data presented in Figures 6 and 8), the X-ray beam was obtained from a sealed tube Cu anode operated at 40 kV and 40 mA, and collimation was effected using a graphite monochromator and a 0.5 mm pinhole collimator. The diffraction pattern was recorded by a two-dimensional gas-filled position-sensitive wire-grid detector. Temperature was controlled by a calibrated Watlow 988 controller and oven supplied by Bruker. The samples were placed in 1.5 mm i.d. Lindemann capillaries (Charles Supper), dried in vacuo for 4 days at 60 °C followed by 2 days at 100 °C, and then sealed (unless otherwise specified).

The *d* spacings were determined from the diffraction peaks using Bragg's relation, $d = \lambda/(2 \sin \theta)$, where 2θ is the diffraction angle and the radiated wavelength $\lambda = 1.542$ nm. Calculated molecular lengths were estimated using Hyperchem 3 (Hypercube Inc.) for the lowest energy conformation of the side-chain or surfactant with all-trans methylene units, including van der Waals radii at the extremities. For the polymer, this length corresponds to the distance from the outermost hydrogen of the methyl group on the polymer backbone to the terminal atom of the side chain.

Preparation of the P12MP-Sp Complexes. The synthesis of the Br^--neutralized parent polyamphiphiles (P12MP-Br), resulting in the formation of gels, is described elsewhere.[10] To avoid gel formation, the polymerizations for the present study were carried out in the presence of a transfer agent, 2-mercaptoethanol (ME), at the ME to monomer (M) molar ratios specified in Table 1; the monomer concentration was 0.2 mol/L, and the initiator to monomer molar ratio was 0.01. Because the polymer is difficult if not impossible to resolubilize once dried,[10] the final purification of P12MP-Br by dialysis[10] was followed directly by the ion-exchange procedure without isolating and drying the polymer. To effect ion-exchange, the dialysis bag containing the purified polymer in water was placed in surfactant-containing solution (aqueous at ambient temperature for S4-Na and S8-Na; water/ethanol (50/50 v/v) at 35 °C for S16-Na). The initial molar concentration of surfactant outside the dialysis bag was about 5 to 10-fold higher than that of the Br^- ions inside the bag. Fresh solution containing the surfactant was renewed seven to eight times during a 5−9-day period. The solvent outside the bag was periodically titrated by silver nitrate, with a yellowish precipitate attesting to the presence of bromide ions. When no further precipitate was detected, the dialysis bag was placed in an aqueous or water/ethanol solution (as above) for 2−6 days, with the solvent changed at least three times daily, to eliminate excess surfactant and Na^+Br^- microions. Finally, the contents of the dialysis bag were freeze-dried (after elimination of most of the ethanol by rotary evaporation for P12MP-S16), followed by vacuum-drying at 70 °C for 2 days before analysis of their purity (if elemental analysis was unsatisfactory, the dialysis procedure was repeated). The freeze-dried fluff was light reddish-brown in color, and tended to be rubbery.

Poly(12-methacryloyloxydodecyl(4-methyl)pyridinium hexadecylsulfonate) (P12MP-S16). ^{1}H NMR ($CDCl_3$, 45 °C): $\delta = 9.30$ [d, 2H, pyridinium in α position]; 7.89 [d, 2H, pyridinium in β position], 4.75 [t (indistinct), 2H, C**H**$_2$−N$^+$], 3.91 [broad, 2H, C**H**$_2$−O], 2.81 [m, 2H, C**H**$_2$−SO$_3^-$], 2.62 [s, 3H, C**H**$_3$−pyr], 2.01 [broad, 2H, C**H**$_2$−C−N$^+$], 1.79 [m (broad), 2H, C**H**$_2$−C−SO$_3^-$], 1.59 [broad, 2H, C**H**$_2$−C−O], 1.5−1.1 [47H, C**H**$_2$ (backbone, spacer, surfactant) and C**H**$_3$ (backbone)], 0.87 [t, C**H**$_3$ (surfactant)]. Anal. Calcd for [$C_{38}H_{69}NO_5S\cdot 0.5H_2O]_n$: C, 69.25; H, 10.71; N, 2.13; O, 13.35; S, 4.86; S/N, 2.28. Found: C, 68.93; H, 11.07; N, 2.06; O, 13.32; S, 4.91; S/N, 2.38.

Poly(12-methacryloyloxydodecyl(4-methyl)pyridinium octylsulfonate) (P12MP-S8). Anal. Calcd for [$C_{30}H_{53}NO_5S$, 1.0 $H_2O]_n$: C, 64.59; H, 9.94; N, 2.51; O, 17.21; S, 5.74; S/N, 2.28. Found for [ME]/[M] = 0: C, 65.10; H, 9.93; N, 2.49; O, 16.61; S, 5.53, Br, 0.35; S/N, 2.22. Found for [ME]/[M] = 0.07×10^{-2}: C, 65.08; H, 9.94; N, 2.49; O, 16.53; S, 5.99, Br, 0.04; S/N, 2.41. Found for [ME]/[M] = 0.1: C, 64.85; H, 9.96; N, 2.51; O, 17.64; S, 5.76; Br, not measured; S/N, 2.29.

Poly(12-methacryloyloxydodecyl(4-methyl)pyridinium butylsulfonate) (P12MP-S4). Anal. Calcd for [$C_{26}H_{45}NO_5S$, 1.0 $H_2O]_n$: C, 62.50; H, 9.48; N, 2.81; O, 19.21; S, 6.40; S/N, 2.28. Found: C, 62.45; H, 9.45; N, 2.71; O, 19.39; S, 6.22, Br, 0.98; S/N, 2.30.

Results

Purity and Solubility of the Complexes. Elemental analysis gives very satisfactory results when specific amounts of residual water are included in the calculated

Table 1. Solubility of P12MP-Br and the P12MP-Sp Complexes in Some Common Solvents[a]

polymer	[ME]/[M][b] ×10²	CH_3OH, CH_3CH_2OH	CF_3CH_2OH	$CHCl_3$	H_2O[c]	$HCONH_2$
P12MP-Br	0	−	−	−	−	−
	6	−	−	−	−	−
	10	−	−	−	−	−
P12MP-S4	6	+	+	−	+	+
P12MP-S8	0	±	±	nt	±	nt
	0.07	±	nt	−	nt	+
	10	+	+	−	+	+
P12MP-S16	6	+	+	+	+	+

[a] Visual observations for about 1% concentration: −, not soluble; ±, slightly soluble; +, soluble; nt, not tested. [b] Molar ratio of transfer agent, ME, to monomer, M. [c] See text for observations at a higher concentration.

values. The agreement between the calculated and experimental S/N ratios is especially significant, since S and N are found exclusively in the surfactant and polymer components, respectively. The presence of residual water is expected given the hygroscopic nature of the materials, and is generally observed for polyamphiphiles[13] and other ion-containing polymers.[14] EDX microanalysis showed no indication of residual sodium or bromine ions, and the SEM images indicated amorphous-looking materials (with lamellar-like appearance). In the ^1H NMR spectra (verified in $CDCl_3$ for P12MP-S16 and in D_2O for P12MP-S8 and P12MP-S4), no visible signal between 5.4 and 6.2 ppm was observed, indicating the absence of residual monomer. In the P12MP-S16 spectrum, it could also be observed that the integrations of the isolated signals for the two components of the complex—in particular, the α and β pyridinium doublets of the polymer vs the $CH_2SO_3^-$ signal of the surfactant—correspond to quantitative substitution of the bromide counterions by octylsulfonate (the spectra for P12MP-S8 and P12MP-S4 in D_2O were of poorer quality, possibly due to aggregation or micelle formation in water; see below). From all of these verifications, it can be concluded that the ion-exchange dialysis method used led to the desired pure and stoichiometric complexes.

The solubility of the complexes was tested qualitatively (by visual observation) in a number of common solvents at a concentration of about 1%, as shown in Table 1. The general insolubility of the parent polyamphiphile was previously reported, and was tentatively attributed to the combined effects of molar mass and amphiphilic character or to very light cross-linking.[10] Table 1 indicates that the polymer remains insoluble in the solvents tested, even for polymerizations in the presence of the transfer agent ME (verified for [ME]/[M] up to 0.1), which presumably results in reduced molar mass.[15] By contrast, the P12MP-Sp complexes show significantly better solubility. For polymerizations in the presence of substantial transfer agent ([ME]/[M] = 0.06−0.1), the complexes appeared soluble in H_2O, alcohols (methanol, ethanol, trifluoroethanol), and formamide. This solubility was reduced for polymerizations with no or very little transfer agent present (tested for P12MP-S8). In $CHCl_3$, a less polar solvent, only the complex with the longest surfactant, P12MP-S16, is soluble. It was also found that, at higher concentrations in water, the complexes have foamlike properties, which appear to be more pronounced the longer the surfactant counterion.

These observations can be compared to those obtained for stoichiometric polyelectrolyte−surfactant complexes, which were also found to be soluble in (organic) solvents in which the parent polymers are not.[7,16−18] On the other hand, whereas water-soluble polyelectrolytes become insoluble in water when stoichiometrically complexed with oppositely charged surfactants (of sufficient length),[7,19] the water-insoluble polyamphiphiles of this study become water-soluble (at low concentrations) when complexed with the surfactants. A possible explanation is that, with small counterions like Br^-, the (aromatic) ionic groups of the polyamphiphile may be "buried" within a strongly interacting hydrophobic agglomeration, whereas, with the surfactant counterions, not only is the sulfonate moiety larger (reducing the strength of the ionic interactions) but the alkyl tail may associate with the alkyl spacer of the polyamphiphile, thereby penetrating the hydrophobic regions and further loosening the strong interactions. The ionic groups, which are far from the polymer backbone, can then be sufficiently exposed to the aqueous medium to allow solubilization in water, like for other tail-end polyamphiphiles.[13,20] The larger size of the sulfonate moiety compared to the Br^- anion may also be a factor.

Thermal Characterization. The thermal stability of the P12MP-Sp complexes was verified by TGA, and compared with that of the parent P12MP-Br. Weight loss thermograms are illustrated in Figure 2, and the temperatures at 5% weight loss are given in Table 2. The data show that the P12MP-Sp complexes are more thermally stable than P12MP-Br by about 70 °C, indicating a dependence of the thermal stability on the nature of the counterion. There is little dependence on the alkyl chain length. Otherwise, the TGA thermograms of the complexes and P12MP-Br are similar in form, with degradation occurring in a first major step followed by a second minor step. The slight slope in the plateau region before degradation may be attributed to the slow removal of residual, strongly bound water.

DSC thermograms of the complexes are compared with that of P12MP-Br in Figure 3, and the associated data are given in Table 3. The Na-neutralized surfactants are all crystalline at ambient temperature, with S4-Na and S8-Na melting above 300 °C (according to the supplier). In fact, S8-Na and S16-Na (S4-Na was not investigated) exhibit a complex thermotropism with at least two intense first-order transitions, of which the first occurs at 180 and 182 °C for S8-Na and S16-Na, respectively.[21] The complexes display quite different behavior. P12MP-S4 and P12MP-S8, in particular, give thermograms with glass transitions (T_g) only and no first-order transitions, thus resembling P12MP-Br. P12MP-S16, on the other hand, displays first-order transitions at temperatures very different from those of S16-Na: a relatively intense transition is observed at 112 °C (several degrees higher in the first scan; see Table 2) and a weaker one occurs at 162 °C on heating. The former shows about 10 °C supercooling and the latter no supercooling, when considering the onset temperatures. As will be shown by X-ray diffraction,

Table 2. Thermal Data for P12MP-Br and the P12MP-Sp Complexes Dried near 100 °C: Degradation Temperature, T_d; Lower and Upper Glass Transition Temperatures, T_g^L and T_g^U; Corresponding Heat Capacity Increments, ΔC_p^L and ΔC_p^U; Melting (or *Crystallization*) Temperature, T_M, and Enthalpy, ΔH_M; Mesophase−Isotropic Phase Transition Temperature, T_I, and Enthalpy, ΔH_I

polymer	T_d (°C)	T_g^L (°C)	ΔC_p^L (J·K·g^{-1})	T_g^U (°C)	ΔC_p^U (J·K·g^{-1})	T_M (°C) (ΔH_M (J/g))	T_I (°C) (ΔH_I (J/g))
P12MP-Br[a]	215	56 ± 3	0.26 ± .03	∼85	∼0.02		
P12MP-S4	290	18	0.32	58	0.08		
P12MP-S8							
[ME]/[M] = 0	275	22	0.33	75	0.14		
[ME]/[M] = 7·10^{-4}		27	0.32	83	0.19		
[ME]/[M] = 0.1		21	0.32	67	0.18		
P12MP-S16	295	17[b]	0.04			112 (14)[b]	162 (3.5)
						93 (−11)[c]	155 (−3.8)[c]

[a] The DSC data for P12MP-Br were obtained from the second and third scans (after quenching) of six different batches polymerized in the presence of variable amounts of 2-mercaptoethanol, ME, ranging from 0 to 0.1 molar ratio of ME relative to monomer, M; no dependence of T_g^L or ΔC_p^L on the ME concentration was evident; the T_g^U and ΔC_p^U values are very approximate due to the poor definition of this transition. [b] Obtained from second, third, and fourth heating scans, after both quenching and slow cooling; on the first scan, the (very weak) T_g appeared to be near 60 °C, T_M = 118 °C, and ΔH_M = 6 J/g, whereas T_I and ΔH_I were the same as in subsequent scans. [c] Cooling thermograms.

Table 3. X-ray Scattering Data Obtained for P12MP-Br and the P12MP-Sn Complexes at Selected Temperatures (Corresponding to the Profiles Shown in Figures 4−6, Unless Otherwise Noted): l_S, Calculated Molecular Lengths for the Surfactant Counterions in All-Trans Conformation; d_1 and d_2, Bragg Spacings Determined from the First and Second Small-Angle Diffraction Peaks, Respectively; amb. 1 and amb. 2, Ambient Temperature Data before and after Heating, Respectively

polymer	temp (°C)	l_S[a] (Å)	d_1 (Å)	d_2 (Å)
P12MP-Br[b]	amb.	3.9	35.0	17.7
P12MP-S4	amb. 1	9.2	∼33	17.0
	amb. 2		∼32	16.7
	90		∼32	16.2
	120		∼30	15.3
P12MP-S8	amb. 1	14.3	31.8	17.3
	amb. 2		31.4	17.0
	50		31.1	16.9
	50[c]		34.0	17.3
	50[d]		35.1	17.8
	90		∼27	15.5
	120		∼25	∼15
P12MP-S16	amb. 1	24.4	36.3	17.8
	amb. 2[e]		35.5	17.7
	130		31.3	15.7
	175		27.5	∼14

[a] The calculated molecular length of the extended polymer repeat unit is 27.3 Å. [b] Data reported in ref 10 for a sample dried in vacuo at 60 °C. [c] Data obtained from a sample dried for several days near 60 °C and overnight near 80 °C. [d] Data obtained from a sample exposed to ambient air for an undetermined period. [e] Noncrystallized (top curve of Figure 7).

these are transitions from an ordered phase at lower temperatures to a disordered liquid crystalline phase at intermediate temperatures to the isotropic phase above the highest transition.

For P12MP-S4 and P12MP-S8, a prominent glass transition is located near 20 °C, with a heat capacity jump (0.3 J·K·g^{-1}) that is similar to that for P12MP-Br. A glass transition at a similar temperature is visible in the thermogram of P12MP-S16, but it is much weaker, which is consistent with crystallinity in the sample as will be discussed below. Thus, all three complexes have a T_g that is 35−40 °C lower than that of P12MP-Br, indicating a similar plasticization effect of the surfactant counterions irrespective of their alkyl chain length.

Another (weaker) T_g-like transition can be observed in the 60−80 °C range for P12MP-S4 and P12MP-S8. The heat capacity increment is greater for the S8 complex than for the S4 complex. This trend as a function of alkyl tail length suggests that a very weak heat capacity increment which can be discerned near 85 °C in the thermogram of P12MP-Br and which can also be detected in those of other similar polyamphiphiles[10] is likewise a T_g-like transition in these materials. It appears broader than the lower temperature T_g. Furthermore, this transition, like the lower one, decreases significantly in temperature when Br^- is replaced by the sulfonate counterions, apparently more for S4 than for S8 (it might be affected as well by factors such as molecular weight or specific sample history, judging from the variation shown in Table 2 for different S8 samples). The presence and possible assignments of the two T_g's or T_g-like transitions will be discussed below (referred to henceforth as the lower and upper T_g's, or T_g^L and T_g^U, respectively).

It should be added that an endothermic peak (up to ca. 3−4 J/g in intensity) just above the upper T_g could be observed in the first heating scan of the P12MP-S8 complex after some time of annealing. The fact that it could also be observed after annealing in the DSC cell (e.g., for about 1 h at 70 °C) following previous scans precludes its attribution to H_2O desorption. The lack of evidence of order after annealing in X-ray diffractograms argues against it being a phase transition. Therefore, it is thought to be an enthalpy peak associated with the upper T_g. A DDSC experiment showing the phenomenon is presented in Figure 4 for a sample annealed overnight at 60 °C in the DSC cell (following previous scans). The endothermic peak is present only in the "loss" C_p component, whereas both glass transition-like events are clearly visible in the "storage" C_p component (with the lower glass transition about twice as intense as the higher one).

Structural Analysis. The ambient-temperature X-ray diffractograms of the P12MP-Sp complexes are compared with that of P12MP-Br in Figure 5, and corresponding data are given in Table 3. It can be observed, first of all, that the X-ray profiles of P12MP-S4 and P12MP-S8 are similar to that of P12MP-Br. In particular, the broad halo near 20° (2θ) indicates the absence of any crystalline order. In contrast, the profile of P12MP-S16 shows the presence of sharper reflections superposed on the wide-angle halo, indicating the coexistence of ordered (crystalline) and disordered structure. A simplistic calculation based on the area of the peaks relative to the total area (peaks and halo)

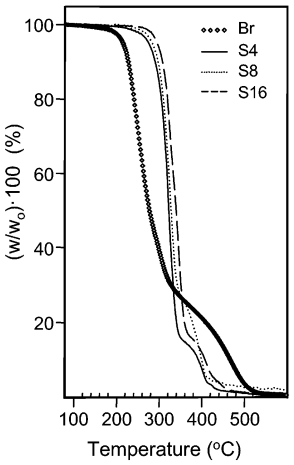

Figure 2. Thermogravimetric scans of P12MP-Br and the polyamphiphile−surfactant complexes, with the counterions indicated.

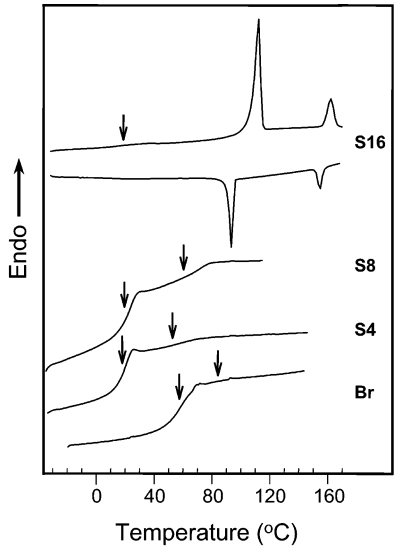

Figure 3. DSC thermograms of P12MP-Br and the polyamphiphile−surfactant complexes, with the counterions indicated (second or higher heating scans).

indicates approximately 15% crystallinity. In the low angle region, there are two essentially equidistant reflections for all three complexes, observed also for P12MP-Br and suggesting lamellar order (see below for more details on the specific case of the S8 complex). The relative broadness of the low-angle reflections indicates that the correlation length of this structure is low for P12MP-Br and P12MP-S4. The greater sharpness and intensity of the reflections for P12MP-S8 is consistent with an increase in correlation length, whereas the sharpness of the reflections for P12MP-S16 can be associated with its partially crystalline character. It is noteworthy that, in contrast to the S16 complex, the first low-angle reflection is less intense than that of the second one for P12MP-Br and the S4 and S8 complexes; this might arise from interference effects of an additional intralamellar plane of symmetry[22,23] such as the presence of a double ionic plane.[24]

Diffractograms of the complexes at higher temperatures are given in Figures 6 and 7. Those for the S4 and S8 complexes in Figure 6 (shown only at lower angles; at wide angles, a halo is observed at all temperatures) indicate, by the decrease in intensities and increase in widths of the low-angle reflections, that the correlation length of the (presumably lamellar) order decreases significantly above about 110 and 70 °C, respectively. This corresponds to the temperature region where the two complexes gradually lose most or all of the birefringence observed between crossed polarizers (the S8 complex maintains slight birefringence up to degradation). In comparison, P12MP-Br was observed to be more weakly birefringent than the complexes, but to lose this birefringence at a higher temperature (near 130 °C).[10] Although the transformation occurs in the region of the upper T_g for the S8 complex, it occurs at higher temperatures than the upper T_g for the S4 complex. On the other hand, the decrease in temperature range of the transformation with increase in counterion size for the three samples (Br, S4, S8) suggests a relationship with the latter parameter. The transformation is reversible, as shown by the return of birefringence and by the reappearance of distinct small-angle reflections in the X-ray diffractograms on cooling. However, it is unaccompanied by a DSC transition, as was also observed for various Br-neutralized polyamphiphiles.[10] This has previously been rationalized by a progressive decrease in size or correlation length of the ordered structure to below the wavelength of visible light.[10,25]

When the S16 complex is heated to the temperature region between the two first-order transitions (130 °C diffractogram in Figure 7), the wide-angle reflections present at lower temperatures disappear, resulting in a simple diffractogram with a wide-angle halo and two equidistant small-angle reflections. This diffractogram is similar to those obtained at ambient temperature for the S4 and S8 complexes, except for the inversion in the relative intensities of the small-angle reflections. It also indicates that the phase between the two DSC transitions is a disordered thermotropic mesophase, probably of the lamellar smectic A or C type. A 2D diffractogram of an oriented sample obtained by manual stretching indicates orthogonal or smectic A order. Between crossed polarizers, this phase is birefringent with a fine-grained texture; it also has significant liquid character, becoming increasingly mobile as the temperature is raised (in contrast, the S4 and S8 complexes remain highly viscous until degradation). Above the higher DSC transition temperature, the sample flows and is optically isotropic between crossed polarizers. The X-ray diffractogram in this phase (170 °C curve in Figure 7) indicates that some order is maintained over very short correlation lengths (as for the other two complexes). The 140 °C curve in Figure 7 shows that the sample returns to the mesophase on cooling, as expected. However, contrary to the DSC result, it did not recrystallize on return to the ambient, possibly because of the comparatively long time spent in the isotropic phase during the X-ray experiment (which may have induced slight degradation that interferes with crystallization or which may have effaced a memory effect that could be present under the DSC conditions). For a sample subjected to less elevated temperatures, recrystallization during cooling was observed (see Figure 8).

It is striking that the Bragg spacings determined from the small-angle reflections are hardly modified by the change in counterion: compared to a spacing of 35 Å for P12MP-Br (probably slightly less if the sample had been dried at the higher temperatures used for the complexes of this study, as indicated in ref 10 for a

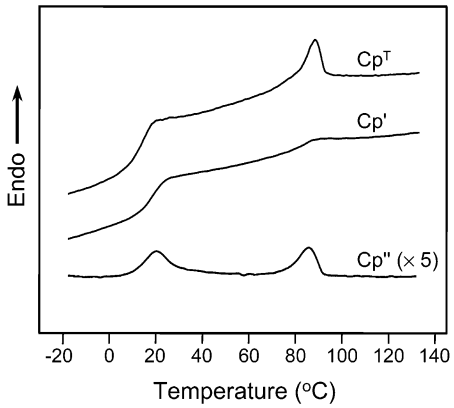

Figure 4. Dynamic DSC of a P12MP-S8 sample that was annealed overnight at 60 °C under dry helium in the DSC sample compartment following previous scans.

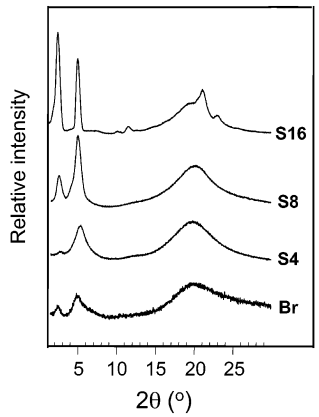

Figure 5. Ambient temperature X-ray diffractograms of P12MP-Br and the polyamphiphile−surfactant complexes, with the counterions indicated.

similar polyamphiphile), that for the complexes ranges from about 31 to 36 Å. This contrasts with the strong increase observed as a function of the alkyl spacer length in the polymer (the Bragg distance doubles for 16 compared to 8 methylene groups in the spacer[10]). In addition, the Bragg spacings for the partially crystalline and the noncrystalline phases of the S16 complex at ambient temperature—bottom and top curves of Figure 7—are almost identical at 35−36 Å. All this suggests that the alkyl tails of the surfactants are somehow accommodated within the basic morphology of the parent P12MP-Br polyamphiphile, for which an orthogonal partial bilayer structure involving interdigitation of the pyridinium moieties was proposed.[10] This will be discussed below.

When the temperature is increased, the Bragg spacings of the S4 and S8 complexes (corresponding to the curves of Figure 6) decrease at a rate of about 0.02 and 0.04 Å/°C, respectively. This effect is typically observed for orthogonal layer structures and is generally attributed to increasing disorder introduced by increasing thermal motion. It may also be noted that the spacing tends to be slightly lower after exposure to high temperatures, which may be related to loss of residual water during heating or to slow thermal equilibrium on recooling. The influence of drying conditions, which presumably affects the amount of residual water (with possible simultaneous annealing effects), is illustrated by the three entries for the 50 °C data of the S8 complex in Table 3 showing the decrease in the Bragg spacing with increased drying. A similar decrease in lamellar

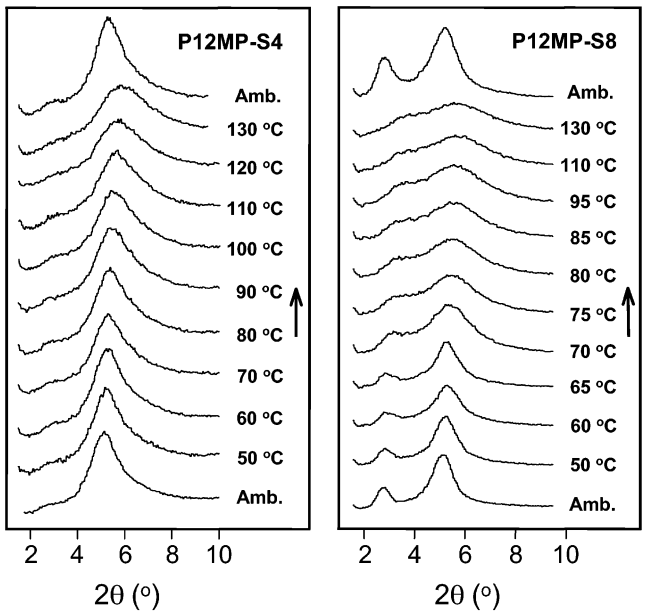

Figure 6. X-ray diffractograms in the small angle region of the P12MP-S4 and P12MP-S8 complexes at the temperatures indicated, taken in order from bottom to top.

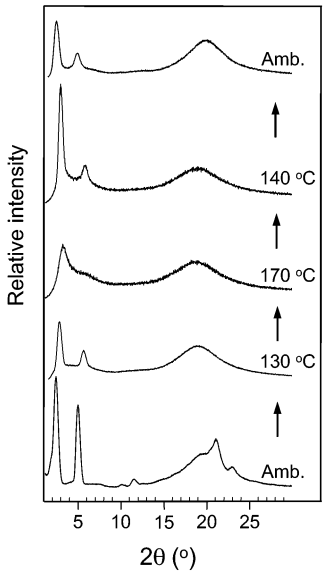

Figure 7. X-ray diffractograms of the P12MP-S16 complex, dried at 100 °C, at the temperatures indicated taken in order from bottom to top.

spacing after more rigorous drying was observed for the Br-neutralized polyamphiphiles.[10]

At this point, it should be remarked that the two small-angle reflections in the profiles of Figure 6 for the well-dried S8 complex are not exactly equidistant; instead, the reciprocal spacings are in a ratio of 1.85, which cannot be accounted for by the uncertainty in the peak maxima. Furthermore, this ratio appears to decrease with increasing temperature (see Table 3). The reflections for the less dry samples, on the other hand, are equidistant within acceptable error (shown in Table 3 for profiles obtained at 50 °C), but their ratios likewise appear to diminish at high temperatures (studied at

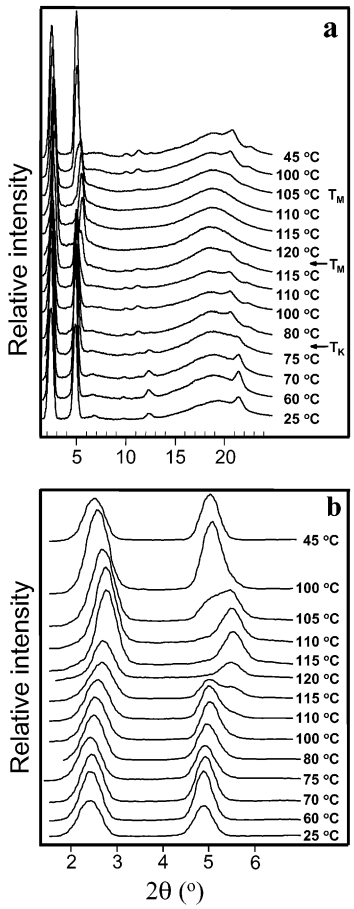

Figure 8. X-ray diffractograms of the P12MP-S16 complex, dried at 60 °C, at the temperatures indicated taken in order from bottom to top. The small angle region of the curves in part a are expanded in part b.

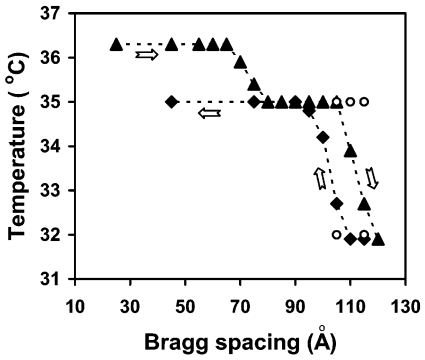

Figure 9. Bragg spacings as a function of temperature for the P12MP-S16 complex, determined from the curves of Figure 8: ▲, heating; ◆, cooling; ○, from two distinct second-order peaks. The arrows indicate the temperature sequence.

only a few temperatures). A plausible explanation for the nonequidistant reflections in the most rigorously dried sample is that the (local) molecular order is not lamellar at the drying temperature used (about 100 °C) and that the cooling rate after drying was more rapid than the time needed to return to lamellar ordering. It is significant that the drying temperature of 100 °C is also in the range where the S8 complex is essentially nonbirefringent. In contrast, the S4 complex is still birefringent with apparent local lamellar order at 100 °C (although the indistinctness of the first-order reflection causes significant uncertainty), which may account for the absence of a similar effect in this complex.

In the S16 complex, the Bragg spacing also decreases somewhat at higher temperature (Table 3). Since at least one phase change is involved, a series of diffractograms were obtained at more closely spaced temperatures, shown in Figure 8. The Bragg spacings determined from the small-angle reflections are plotted in Figure 9 as a function of temperature. The latter figure shows that the Bragg spacing changes by about 3 Å at the crystal-mesophase transition, and is reversible on cooling (with a thermal lag of about 10 °C). Such a decrease at the transition is expected if crystalline chains melt, i.e., become disordered, with no other changes in their longitudinal packing. The small decrease in lamellar spacing at lower temperatures will be discussed below.

Significantly, whereas the superposition of the crystalline peaks and amorphous halo at wide angles indicates partial crystallinity in this complex below the crystal−mesophase transition, there is no evidence in the small-angle region of superposition of different mesophase and crystalline reflections at low temperature. On the other hand, distinct small-angle reflections for the two phases are clearly visible within the transition region (the 115 °C curve on heating and the 105 °C curve on cooling in Figure 8) where the two phases are simultaneously present and are obviously characterized by somewhat different *d* spacings. The absence of two distinct *d* spacings at lower temperatures thus suggests that the partial crystallinity in the sample does not arise from a fraction of the side chains that are crystallized and another fraction that maintain the higher temperature mesophase structure (i.e., are not crystallized). Instead, it likely arises from surfactant alkyl tail-ends that are more or less uniformly crystallized throughout the material, with the wide angle halo resulting primarily from the disorder in the inner portion of the complexed side chains. It is well-known that aliphatic side-chain polymers exhibit crystallinity only when the side chains are sufficiently long that their ends are free from the constraints imposed by the polymer backbone—i.e., decoupled from the main-chain—so that crystallization of the ends becomes possible.[26] This is observed for both covalently[26,27] and noncovalently[28−30] grafted side chains. The resulting structure can be envisaged as an alternation of amorphous and crystalline regions along the side-chain axis.[26] In the complexes of the present study, the pyridinium groups similarly impose constraints on crystalline order, and only S16 is sufficiently long to have decoupled tail-ends that can crystallize.

Figure 8 also shows that there is a transition between two different crystalline forms for the S16 complex, with the higher temperature one corresponding to the ambient temperature form shown in Figure 7. The difference in the ambient-temperature diffractograms of the two figures can be related to the drying temperature, which was about 100 °C for Figure 7 and about 60 °C for Figure 8. Concordantly, a DSC thermogram of the latter shows an endotherm at 77 °C (first scan; at 69 °C and much weaker in intensity in a second heating scan following a maximum scan temperature of 140 °C; at 56 °C and weak on cooling). In the ambient temperature diffractogram of the complex dried near 60 °C (Figure 8), a single wide-angle reflection, which is located at 21.5° (4.13 Å) and which can be attributed to hexagonal packing within lamellar planes[29,30] (smectic B-like if orthogonal layers are assumed), is superposed on the

wide-angle halo. The ambient temperature diffractogram of the complex dried near 100 °C (Figure 7) shows two reflections superposed on the halo, a more intense one at 21.1° (4.21 Å) and a weaker one at 23.0° (3.86 Å). This is similar to what is generally reported for orthorhombic packing of alkyl chains (110 and 200 planes) of, for example, polyethylene[31] and aliphatic side chains.[29,30] At temperatures above the crystal−crystal transition (Figure 8), the two wide-angle peaks indicative of orthorhombic packing are located at 20.8° (4.27 Å) and 22.6° (3.94 Å), indicating slight lateral expansion compared to ambient temperature packing that can be attributed to increased thermal motion. The long periods or Bragg spacings of the two crystalline forms are only slightly different, with the orthorhombic form about 1 Å less than the hexagonal form. The lateral molecular areas (unit cell) calculated from these data assuming orthogonal layers are all very similar: 19.7 and 19.4 Å^2 for the ambient temperature hexagonal and orthorhombic packing, respectively, and 20.0 Å^2 for the higher temperature orthorhombic packing. The slightly smaller area and long period for the ambient temperature orthorhombic form compared to the hexagonal form might be explained by the removal of residual water molecules or to improved packing due to effective annealing after exposure to high temperature.

Finally, it is of interest to mention that samples of the S16 complex that were poorly dried or that were stored over long periods in ambient conditions showed more complicated behavior. X-ray diffractograms of a sample that was only freeze-dried suggested a columnar−cubic−lamellar phase sequence on increasing the temperature. The presence of the cubic phase was supported by POM observations that showed a considerable (and reversible) decrease in birefringence when cooling from the higher temperature lamellar-like phase, the residual birefringence suggesting a superposition of lamellar and cubic organization (also consistent with the X-ray data). Analogous observations were made for some polyelectrolyte−surfactant complexes containing equilibrium amounts of water (and which were simply lamellar when thoroughly dry); it was postulated that this is related to local thickness undulations of the lamellar superstructure that pack in a cubic arrangement.[32] These data and those for other less dried alkyl sulfonate−pyridinium amphiphile complexes[24] will be presented and discussed in a future publication.

Discussion

Two T_g's. There have been occasional reports in the literature of two (DSC-detected) T_g's in other comblike polymers, notably by Cowie et al.[33] for poly(di-*n*-alkyl itaconate)s, by Percec and collaborators[34,35] for siloxane-based side chain liquid crystalline (SCLC) copolymers, and by Emmerling et al.[36] for a (wide-toothed) tin-containing SCLC polymer. The presence of two T_g's has been associated with distinct (nano)phase separation between the two parts of the polymer, much as in graft copolymers.[33a,35b] This was considered to be favored in the poly(dialkyl itaconates) by the high density of ester-linked side chains where the ester groups form an impenetrable polar core separate from the alkyl chains,[33] in siloxane-based SCLC polymers by the chemically dissimilar and flexible siloxane backbone compared to the side chains,[34,35] and in the tin-containing polymer by the location of the Sn atom in the backbone enhancing its immiscibility with the side chains.[36] It was noted that similar behavior is not observed in poly(alkyl methacrylate)s, possibly due to less well-defined nanophase separation.[33a,c,37b]

The T_g's were then attributed to cooperative main-chain motion and to cooperative side-chain motion, respectively,[38] the specific assignments depending on the system. For the polyitaconate polymers, the lower and upper T_g's (T_g^L and T_g^U, respectively) were assigned to side-group and main-chain mobility, respectively. For the siloxane-based and Sn-containing SCLC polymers, the reverse assignments were made. Heat capacity variations as a function of side-chain length and/or copolymer composition, as well as dielectric measurements of the Sn-containing SCLC polymer, supported the attributions. In particular, for the poly(itaconate) series, ΔC_p^L increases with increasing side-chain length (of homopolymers) and with increasing content of long side-chain units (of copolymers), whereas ΔC_p^U is constant and decreases, respectively. In the siloxane SCLC polymers, the lower T_g was not detected in copolymers of high mesogenic content (more than 90 wt % or 60 mol %), which was ascribed to the insufficient weight fraction of the backbone. Similarly, a T_g detected near ambient temperature in poly(α-amino acid)s was attributed to the soft side-chain region, with a main-chain T_g thought to be at temperatures beyond the onset of degradation (the main chain being in the form of a rigid helical core).[37,39]

For the materials of the present study, it can be argued that, with reference to the poly(alkyl methacrylate)s where two T_g's are not observed (see above), discrete nanophase separation is not expected to occur between the methacrylate backbone and alkyl spacer. On the other hand, the ionic pyridinium moieties can certainly be envisaged to form a distinct nanophase separate from the nonionic regions of the polymer. Then, by analogy with biphasic (amorphous) ionomers where a lower temperature T_g is associated with a nonpolar or ion-poor (soft) phase and a higher temperature T_g with an ionic or ion-rich (hard) phase,[40] it is conceivable that the pyridinium tail-ends form the harder phase giving rise to the upper T_g. Its being barely visible in the Br-neutralized polymer is consistent with the small fraction of the ionic part compared to the nonionic parts. The increasing ΔC_p of this transition with increase in surfactant length suggests that the surfactant counterions are located in this phase, which in turn can also rationalize the lack of significant influence of the surfactant length on the lower temperature T_g. The latter is then associated with the softer phase composed of the polymer backbone and alkyl spacer. The decrease in the temperature of the lower T_g when Br^- is replaced by the larger sulfonate headgroups might be explained by the somewhat weaker ionic interactions of the latter, which may reduce its rigidity and hence also affect the mobility of the nonionic phase to which the ionic phase is intimately interconnected by covalent bonds. If the assignments are correct, then this explanation of the indirect effect of the ionic phase on the nonionic phase may also be invoked to account for the significant influence of the nature of the pyridinium group on the T_g's in the other pyridinium polyamphiphiles investigated by us.[10] The coupling model considerations of Ngai[41] for thin polymer films (on surfaces or confined between rigid layers) may also be relevant to elucidate the two T_g's. It should be possible, in future work, to

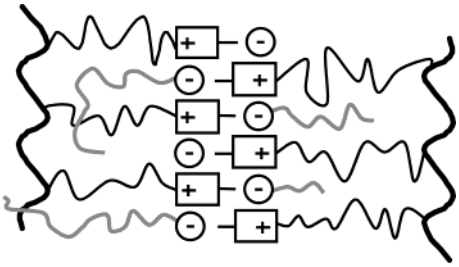

Figure 10. Schematic indicating how the surfactant counterions might be accommodated within the basic molecular structure supposed for the parent P12MP-Br polyamphiphile. One S4, one S8, and two S16 surfactant molecules are represented by the short, medium, and long anion-attached wavy lines, respectively. One S16 molecule is shown to be mixed with the alkyl spacers only and the other with the spacers and backbone.

clarify the identification of the two T_g's by, for example, an investigation of a series of partially ion-exchanged samples of P12MP-Br/S8 copolymers, by dynamic mechanical or dielectric analyses, or by solid-state NMR studies using (partially) deuterated surfactant counterions.

Molecular Organization. Any proposed molecular structure for the dried polyamphiphile/surfactant complexes, which are considered to be organized in orthogonal lamellar form like the Br-neutralized polyamphiphile, must take into account the fact that the *d* spacing is essentially the same as for P12MP-Br and independent of the surfactant length. The structure proposed[10] for P12MP-Br and similar polyamphiphiles, shown in Figure 10, is characterized by interdigitation of the pyridinium moieties in a double ionic subplane. On the basis of this model, it is conceivable that the alkyl tails of the counterions are located within the subplanes formed by the alkyl spacers of the polymer, as also illustrated in Figure 10. This seems particularly reasonable for the S4 and S8 counterions, whose alkyl chains are shorter than the alkyl spacer of the polymer. It may also be possible for the S16 counterion in its noncrystallized form (schematicized in two ways in Figure 10). Given the location of the pyridinium charge on the alkyl spacer side (although the charge may be delocalized to some extent over the ring), this arrangement maximizes segregation between the aromatic and alkyl subplanes. The relative flexibility of the backbone could be a contributing factor that may allow such an accommodation of the surfactants within a basic structure dictated essentially by the polymer.

On the other hand, it seems difficult to rationalize the tail-end crystallinity of the S16 surfactant, along with the invariance of the *d* spacing compared to the noncrystallized form, by the proposed model. A different model that may be considered for the S16 complex is shown in Figure 11. In this model, the surfactant tail is oriented such that it effectively lengthens the polymer side-chain. This easily allows for tail-end crystallization. A local domain of this extended tail-end crystallized complex is represented pictorially in Figure 11a, where the various subplanes (backbone, spacer, ionic, surfactant inner chain, surfactant tail) are distinguished. The isolated lines in the tail-end region represent overlapping tails from a neighboring complex domain (below the one shown), which is flipped in the opposite direction vertically. Although not necessarily essential, the overlapping tails in the crystalline region allow better harmonization of the molecular area of this region with

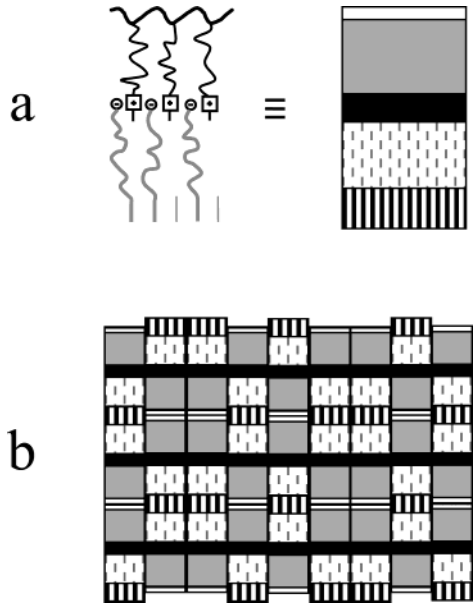

Figure 11. Simplified schematic of an alternative molecular arrangement for the P12MP-S16 complex: (a) pictorial representation of a single complex domain with the different molecular parts distinguished (the two isolated lines in the bottom portion at left represent overlapping tail-ends of a neighboring domain below the one shown and oriented in the opposite direction vertically); (b) possible arrangement of multiple domains, where the ionic sublayers form a continuum and the crystallized tail-end portions of oppositely oriented vertical pairs are overlapped (see text for details).

that of the ionic plane, the disordered alkyl segments of the spacer and surfactant filling in the intermediate volumes appropriately.

Considering that each domain represented in Figure 11a is paired with an oppositely oriented domain (with overlapping of the crystalline tail-end regions), the idealized model shown in Figure 11b may be proposed. In this model, the paired domains are oriented randomly about the ionic subplane such that the ionic subplanes form a continuum, with an interplanar separation that is essentially twice the distance between the polymer backbone and the ionic subplane, as for the model in Figure 10. The domains are shown to be of constant width (or multiples thereof) for ease of representation, but it is more likely that they have variable widths. It so happens that the estimated proportions drawn for the subdomains are such that, with overlapping of the crystalline portions, almost perfect alignment of the ionic sublayers are obtained in Figure 11b. In reality, the true proportions are not known; however, if different from that shown, it would only create a random rippling effect giving an average Bragg spacing. This might explain the slightly greater Bragg spacing obtained for the S16 complex than for the others (Table 3), if the surfactant alkyl subdomain is a little thicker than estimated in Figure 11. Finally, it is significant that this model is characterized by a single ionic layer rather than the double one of Figure 10. This is consistent with the inversion of the intensities of the two small-angle X-ray peaks for the S16 complex compared to the parent polymer and the S4 and S8 complexes, which suggests a significant change in packing normal to the lamellae: that is, a double ionic plane can give rise to an interference effect that reduces the intensity of the first-order reflection (as observed for the parent polymer and

the S4 and S8 complexes), and this is removed by a change to a single ionic plane.[24] Since the intensity ratio for the crystalline and noncrystalline forms of the S16 complex is the same, it may be supposed that the model in Figure 11b is applicable to both forms.

Although the two models discussed seem credible, questions still remain. For example, it might be argued that, for identical packing in the ionic sublayer, the additional volume required by the surfactant tails in the model of Figure 10 would cause an extension of the alkyl segments and hence a thickening of the lamellar planes with increasing surfactant length. It is also not clear that this model is compatible with the proposed assignment for the two T_g's in the S4 and S8 complexes. In particular, if the alkyl tails of the complexed surfactants are mixed with the alkyl spacers of the polymer and thus lie within the alkyl/backbone subplane of the lamellae, it seems curious that the heat capacity of T_g^L, which was assigned to this subphase, remains constant, whereas that of T_g^U, which was assigned to the pyridinium subphase, increases. Thus, further investigation is required to define the molecular organization with greater certitude.

It may be remarked that low molar mass analogues of the present complexes (i.e., alkylpyridinium alkyl sulfates), which were investigated in great detail and determined to have smectic A organization, showed a much weaker dependence of the layer spacing on total complexed molecular length than expected, which could not be rationalized by usual molecular models.[42] Instead, a molecular model of interdigitated and noninterdigitated complexed molecules with the ionic sublayer (of single and double ionic planes, respectively) disposed in incoherent undulations, leading to an averaged interplanar distance in the diffractograms, was proposed. Although this model as such is not applicable to our polymer system, where almost no dependence on surfactant length is observed and where polymer connectivity must be accounted for, it does support the greater complexity in molecular order that seems to be present in these complexed systems. It also has in common with the model of Figure 11 the presence of randomly correlated domains connected via the ionic sublayers.

Conclusions

The polyamphiphile−surfactant complexes investigated self-assemble into supramolecular comblike polymers with the complementary (ionic) interaction far from the polymer backbone. Compared to polyelectrolyte−surfactant complexes, where the ionic interaction is at or near the polymer backbone, this enhances the polymeric character of the material. It also allows novel comblike packing in that the surfactant tail may extend the teeth of the polyamphiphile comb longitudinally, or fold back to mix with the polyamphiphile spacer, or even induce a bend in the teeth if the surfactant connects to the polyamphiphile side chain at some angle other than 0 or 180°.

In the systems studied, the complexes with surfactants that are shorter than the alkyl spacer of the polyamphiphile self-organize as disordered mesomorphic materials, probably with lamellar order of short correlation lengths, similar to the parent bromine-neutralized polyamphiphile. The complexes become optically isotropic at higher temperatures, unaccompanied by a DSC transition. On the other hand, two glass transition-like events are detected by DSC, with the upper one becoming increasingly evident with increase in counterion length. This phenomenon has been reported only occasionally in the literature for similar (comblike) systems. We have tentatively assigned the lower and upper T_g's to nanophase-separated nonionic and ionic lamellar subplanes, respectively.

The complex with the surfactant that is longer than the polyamphiphile spacer displays thermotropic liquid crystalline behavior, with DSC transitions between two partially crystalline forms at low temperature, a smectic A-like phase at intermediate temperatures and the isotropic phase at higher temperatures. The crystallization is thought to occur at the surfactant tail-ends, where there is sufficient decoupling from the ionic charges. Surprisingly, the lamellar thickness is insensitive to the surfactant length and to the presence or not of crystallinity, and is almost identical to that for the parent polyamphiphile. This indicates that the interplay between the polymer backbone and the ionic interactions dominate the molecular packing adopted. Two possible models are proposed to rationalize the observations, the first involving folding back of the surfactant tail within the plane of the polyamphiphile spacer (and possibly backbone), the second involving longitudinal extension of the polyamphiphile side chain (which permits tail-end crystallization) but with random alternation of subdomains and partial overlap of the tail-ends in such a way that the distance between the ionic subplanes is hardly modified.

Acknowledgment. The financial support of NSERC (Canada) and FCAR (Québec) is gratefully acknowledged. We also thank Dr. Jean-Claude Galin, of l'Institut Charles Sadron (ICS), Strasbourg, France, for kindly overseeing the elemental analyses done at ICS.

References and Notes

(1) Lehn, J. M. *Supramolecular chemistry − concepts and perspectives*; VCH: Weinheim, Germany, 1995.
(2) Ikkala, O.; ten Brinke, G. *Science* **2002**, *295*, 2407.
(3) Kato, T. *Struct. Bonding (Berlin)* **2000**, *96*, 95 and references therein. Kato, T. In *Handbook of Liquid Crystals*; Demus, D., Goodby, J. W.. Gray, G. W., Spiess, H., Vill, V., Eds.; Wiley-VCH: Weinheim, Germany, 1998; Vol. 2B, p 969 and references therein.
(4) Ciferri, A., Ed. *Supramolecular Polymers*; Marcel Dekker: New York, 2000.
(5) Bazuin, C. G. In *Mechanical and Thermophysical Properties of Polymer Liquid Crystals*; Brostow, W., Ed.; Chapman and Hall: London, 1998; Vol. 3, Chapter 3 and references therein.
(6) Antonietti, M.; Thünemann, A. *Curr. Opin. Colloid Interface Sci.* **1996**, *1*, 667 and references therein.
(7) MacKnight, W. J.; Ponomarenko, E. A.; Tirrell, D. A. *Acc. Chem. Res.* **1998**, *31*, 781 and references therein.
(8) Zhou, S.; Chu, B. *Adv. Mater.* **2000**, *12*, 545 and references therein.
(9) Tsiourvas, D.; Paleos, C. M.; Skoulios, A. *Macromolecules* **1999**, *32*, 8059.
(10) Vuillaume, P. Y.; Galin, J.-C.; Bazuin, C. G. *Macromolecules* **2000**, *33*, 781.
(11) Exceptionally, a polyamphiphile with a side-chain of 16 methylene units terminated by dimethylaminopyridinium is thermotropic, showing both well-defined melting and clearing points. Vuillaume, P. Y.; Bazuin, C. G. *Am. Chem. Soc. Polym. Prepr.* **1999**, *40* (2), 490 (full publication in preparation).
(12) Calme, P.; Keyzer, M. *Mikrochim. Acta* **1969**, *6*, 1248.
(13) (a) Köberle, P.; Laschewsky, A. *Macromolecules* **1994**, *27*, 2165. (b) Favresse, P.; Laschewsky, A. *Polymer* **2001**, *42*, 2755.
(14) Eisenberg, A.; King, M. *Ion-Containing Polymers*; Academic Press: New York, 1977.
(15) Unfortunately, no easy and reliable method was found to actually determine the molar mass of the polymers,[10] al-

though renewed efforts on another series of pyridinium polyamphiphiles are in progress (Brodin, C. Ph.D. Thesis, Dép. de chimie, Université Laval, Québec, 2003).
(16) Antonietti, M.; Conrad, J. Thünemann, A. *Macromolecules* **1994**, *27*, 6007.
(17) Antonietti, M.; Förster, S.; Zisenis, M.; Conrad, J. *Macromolecules* **1995**, *28*, 2270.
(18) Ponomarenko, E. A.; Tirrell, D. A.; MacKnight, W. J. *Macromolecules* **1996**, *29*, 8751.
(19) Goddard, E. D., Ananthapadmanabhan, K. P., Eds. *Interactions of surfactants with polymers and proteins*; CRC Press: Boca Raton, FL, 1993; Chapter 4, Part II, Chapter 5.
(20) Laschewsky, A.; Zerbe, I. *Polymer* **1991**, *32*, 2070. Bonte, N.; Laschewsky, A. *Polymer* **1996**, *37*, 2011.
(21) DSC thermograms (limited to a maximum temperature of 250 and 200 °C for S8-Na and S16-Na, respectively) combined with X-ray diffractograms obtained at selected temperatures suggest that both surfactants possess a bilayer smectic B mesophase (between 219 and 237 °C on heating for S8-Na) as well as a disordered smectic mesophase (probably smectic A) above 237 and 182 °C for S8-Na and S16-Na, respectively.[24.]
(22) Navarro-Rodriguez, D.; Guillon, D.; Skoulios, A.; Frère, Y.; Gramain, Ph. *Macromol. Chem.* **1992**, *193*, 317.
(23) Tork, A.; Bazuin, C. G. *Macromolecules* **2001**, *34*, 7699.
(24) Vuillaume, P. Y. Ph.D. Thesis, Dép. de chimie, Université Laval, Québec, 2000.
(25) Ponomarenko, E. A.; Waddon, A. J.; Bakeev, K. N.; Tirrell, D. A.; MacKnight, W. J. *Macromolecules* **1996**, *29*, 4340.
(26) Platé, N. A.; Shibaev, V. P. *J. Polym. Sci., Macromol. Rev.* **1974**, *8*, 117.
(27) (a) Lee, J. L.; Pearce, E. M.; Kwei, T. K. *Macromolecules* **1997**, *30*, 6877 and references therein. (b) Watanabe, J.; Ono, H.; Uematsu, I.; Abe, A. *Macromolecules* **1985**, *18*, 2141.
(28) Ponomarenko, E. A.; Waddon, A. J.; Tirrell, D. A.; MacKnight, W. J. *Langmuir* **1996**, *12*, 2169.
(29) Luyten, M. C.; Alberda van Ekenstein, G. O. R.; ten Brinke, G.; Ruokolainen, J.; Ikkala, O.; Torkkeli, M.; Serimaa, R. *Macromolecules* **1999**, *32*, 4404.
(30) Cai, Y.; Wang, D.; Hu, X.; Xu, Y.; Zhao, Y.; Wu, J.; Xu, D. *Macromol. Chem. Phys.* **2001**, *202*, 2434.
(31) (a) Simanke, A. G.; Alamo, R. G.; Galland, G. B.; Mauler, R. S. *Macromolecules* **2001**, *34*, 6959. (b) Baker, A. M. E.; Windle, A. H. *Polymer* **2001**, *42*, 667. (c) Antinucci, S.; Guerra, G.; Oliva, L.; Ruiz de Ballesteros, O.; Venditto, V. *Macromol. Chem. Phys.* **2001**, *202*, 382.
(32) Antonietti, M.; Maskos, M. *Macromolecules* **1996**, *29*, 4199.
(33) (a) Cowie, J. M. G.; Haq, Z.; McEwen, I. J.; Velix̆c4kovi, J. *Polymer* **1981**, *22*, 327. (b) Cowie, J. M. G.; McEwen, I. J.; Pedram, M. Y. *Macromolecules* **1983**, *16*, 1151. (c) Arrighi, V.; Triolo, A.; McEwen, I. J.; Holmes, P.; Triolo, R.; Amenitsch, H. *Macromolecules* **2000**, *33*, 4989.
(34) Hsu, C. S.; Percec, V. *Makromol. Chem., Rapid Commun.* **1987**, *8*, 331. Hsu, C. S.; Percec, V. *Polym. Bull. (Berlin)* **1987**, *17*, 49 and *18*, 91.
(35) (a) Hahn, B.; Percec, V. *Macromolecules* **1987**, *20*, 2961. (b) Percec. V.; Hahn, B. *Macromolecules* **1989**, *22*, 1588. (c) Percec. V.; Hahn, B.; Ebert, M.; Wendorff, J. H. *Macromolecules* **1990**, *23*, 2095.
(36) Emmerling, U.; Lindau, J.; Diele, S.; Werner, J.; Kresse, H. *Liq. Cryst.* **2000**, *27*, 1069.
(37) (a) Tsutsumi, A.; Hikichi, K.; Takahashi, T.; Yamashita, Y.; Matsushima, N.; Kanke, M.; Kaneko, M. *J. Macromol. Sci.—Phys.* **1973**, *B8*, 418. (b) Yamashita, Y.; Tsutsumi, A.; Hikichi, K.; Kaneko, M. *Polym. J.* **1976**, *8*, 114. (c) Sugai, S.; Kamashima, K.; Makino, S.; Noguchi, J. *J. Polym. Sci., Part A-2* **1966**, *4*, 183.
(38) For alternative explanations, and arguments against them, see ref 35b.
(39) Pezzin, G.; Ceccorulli, G.; Pizzoli, M.; Peggion, E. *Macromolecules* **1975**, *8*, 762.
(40) Eisenberg, A.; Kim, J. S. *Introduction to Ionomers*; John Wiley & Sons: New York, 1998.
(41) Ngai, K. L. *J. Phys. Chem. B* **1999**, *103*, 5895. Ngai, K. L. *Eur. Phys. J. E* **2002**, *8*, 225.
(42) Cruz, C.; Heinrich, B.; Ribeiro, A. C.; Bruce, D. W.; Guillon, D. *Liq. Cryst.* **2000**, *27*, 1625.

MA0344442